Image-based visual servoing through micropart reflection for the microassembly process

2011 J. Micromech. Microeng. 21 065016

(http://iopscience.iop.org/0960-1317/21/6/065016)

J. Micromech. Microeng. **21** (2011) 065016 (12pp) doi:10.1088/0960-1317/21/6/065016

Image-based visual servoing through micropart reflection for the microassembly process

Henry K Chu, James K Mills and William L Cleghorn

Department of Mechanical and Industrial Engineering, University of Toronto, 5 King's College Road, Toronto, Ontario M5S 3G8, Canada

E-mail: chu@mie.utoronto.ca, mills@mie.utoronto.ca and cleghrn@mie.utoronto.ca

Received 18 January 2011, in final form 9 March 2011
Published 4 May 2011
Online at stacks.iop.org/JMM/21/065016

Abstract

This paper presents an image-based visual servoing algorithm to perform the microassembly process with an uncalibrated manipulator. The proposed algorithm requires only the use of the visual information from a single-vision camera to evaluate the unknown Jacobian matrix. Two methodologies were examined to estimate the Jacobian matrix on-line. Through monitoring the selected feature and the image reflection from the surface, the 3D position between the slot and the micropart can be evaluated successfully for the assembly process. Experimental results confirmed that the Jacobian matrix computed from both methods can evaluate the position with an accuracy of 3.6 μm initially. By using a proportional gain control, the position accuracy can be improved to within 1 μm. Measurement noise during the image acquisition is determined to be one of the root causes of the evaluation accuracy.

(Some figures in this article are in colour only in the electronic version)

1. Introduction

The recent advancement in micro technology has inspired engineers to develop new and more functional MEMS devices to better serve our daily lives. MEMS sensors and actuators have been featured in many consumer products to enhance performance and functionality. MEMS-based motion sensors and touch-screen sensors integrated in many handheld devices and electronics are examples of these MEMS applications.

During the design and development phase of a novel MEMS device, the available micro-fabrication methodology usually limits the complexity of the proposed MEMS device. To date, many of these micro-fabrication methodologies can be categorized as either surface micromachining or bulk micromachining. Surface micromachining is used to fabricate MEMS devices by depositing multiple thin films onto the wafer, while bulk micromachining is used to fabricate MEMS devices by etching away the unwanted parts from the wafer. The design layers used for deposition or etching in both methodologies are essentially two dimensional. Hence, MEMS devices are often referred to as 2-1/2D structures. In order to fabricate complicated, 3D MEMS devices, microassembly is one of the promising approaches to resolve the issue.

Microassembly is the process of manipulating and assembling micro-components in the micro-world environment. The typical dimensions of the micro-component typically range from tens to several hundred microns [1]. To achieve high precision in handling and positioning these micro-components, robotic manipulators are often used to perform the microassembly process. These manipulators are usually equipped with one- or multiple-vision cameras to provide visual feedback during the process. With the visual information, the exact position and the orientation of the micro-components can be evaluated and used to develop the controller inputs of the manipulator. The use of visual information to control the motion of a manipulator is also known as visual servoing.

In summary, visual servoing can be grouped into two types: position-based visual servoing and image-based visual servoing. In position-based visual servoing, object features are extracted from the image and used to estimate the object's position and orientation. The controller inputs of

the manipulator are then developed based on the difference between the desired and the current manipulator positions in the task space. In image-based visual servoing, the evaluation and the control schemes are typically developed in the image space. The desired motions of the manipulator in the image space are coordinated through an image Jacobian matrix. An in-depth discussion of these two visual servoing techniques can be found in [2].

Both visual servoing techniques have been adopted in practice in many macroscopic applications [3–5]. Recently, the research on visual servoing techniques has been extended to the microscopic world for microassembly processes. For example, Feddma *et al* [6, 7] applied an image-based visual servoing technique to assemble LIGA parts. CAD drawings of the parts were used to create synthetic images and these images were applied to visually servo the LIGA part to the desired position. Ralis *et al* [8] proposed a visual servoing framework for assembly and packaging of MEMS. The probe of the manipulator was successfully manipulated to the specified target hole through multiple-vision sensors. Wang *et al* [9] performed a micropeg-in-hole operation with visual servoing. Kalman filtering was employed to estimate the Jacobian matrix and the hole was manipulated and aligned with the peg through visual images.

For the above microassembly processes, the end-effectors of the manipulators are very small in size due to the delicate nature of the micro-components. Hence, the eye-to-hand configuration is adopted for the vision system. Vision cameras are mounted separately on a fixed stand to provide a panoramic view of the end effectors. In many cases, the end-effector is observed directly from the overhead camera. With such a configuration, the visual servoing task is straightforward since the image plane is co-planar with one of the motion planes of the manipulator. Two-dimensional images from the vision cameras are used to evaluate the necessary planar motions of the manipulator. The motion along the out-of-plane direction, which cannot be observed from the overhead image, can be evaluated using algorithms such as image sharpness [6], active zooming [10] or stereo images [11].

When the assembly tasks become more complicated, images from the overhead camera may not always be the best viewing angle as the objects of interest could be occluded or invisible to the camera. Positioning the vision camera to provide isometric or trimetric images may better observe the assembly process. Nevertheless, the available 2D visual information from a single-vision camera may not be adequate to evaluate the true 3D position, i.e. the end-effector at a particular coordinate in the image could be represented by multiple positions in the task space. Hence, researchers developed different methodologies to determine the true 3D position for visual servoing through a single-vision camera. For instance, Yesin *et al* [12] and Tamadazte *et al* [13, 14] proposed the use of CAD models to perform 3D visual tracking. CAD models of the micro-components are loaded and rendered into the captured images for feature extraction and transformation matrix estimation. Mikawa *et al* [15] and Kulpate *et al* [16] used reflective images from mirrors as an additional feature point for visual servoing. The reflection from the mirrors is captured and used to evaluate the depth information or 3D position information.

In this work, an image-based visual servoing algorithm was developed to perform the 3D microassembly process through an uncalibrated robotic manipulator. The assembly task is similar to a peg-in-hole process and the micro-component must be inserted into the slot. However, the peg on the micro-component is occluded by the body structure when viewing from the overhead camera. Hence, a single-vision camera with a trimetric-view configuration is used to provide the necessary visual information for servoing. In this work, the concept of using mirror reflection in macroscopic assembly processes [15, 16] is applied to the proposed microassembly process. Compared to the CAD-model approach discussed in [12–14], this servoing algorithm is able to function in an uncalibrated environment since this approach does not require previously calibrated camera parameters to render the CAD model of the micro-component to the estimated pose for servoing. The true 3D position difference between the micro-component and the slot is evaluated by monitoring the micro-component and its reflection in the images. Silicon is selected as the fabrication material of the micro-component. Since silicon possesses high reflectivity like other metals, additional mirrors are not required to be installed onto the manipulator and the micro-component reflection on the slot surface is used for the computation. The proposed algorithm then automatically re-positions the slot to the desired position for the assembly process.

The proposed microassembly process was conducted using an in-house six-DOF manipulator at the Nonlinear System Control Laboratory, University of Toronto. Chu *et al* successfully designed the microgripper and the mechanical joint for use in this microassembly process [17, 18]. The algorithms developed in [19, 20] can automatically align and position the micro-component, at any arbitrary orientation initially, with the microgripper for grasping. The visual servoing scheme contribution presented in this research is toward the automation of the insertion operation for the ongoing parallel microassembly research.

This paper is organized as follows. Section 2 reviews the process of the microassembly and the robotic manipulator. Details on the construction of the image Jacobian matrix are presented in section 3. Section 4 provides the experimental results and discussion on this work. Section 5 concludes the work and gives the future direction of our work.

2. Background

2.1. Six-DOF manipulation system

The robotic manipulator used for the microassembly process is shown in figure 1. Similar to other micromanipulators or probe stations available in the market, this manipulator consists of a movable worktable and an end-effector. The worktable can translate along the x-, y- and z-axes through the translation stages and can also rotate along the α-axis. The end-effector is equipped with a tungsten probe and it can provide two degrees of rotational motions to the tip of a tungsten probe.

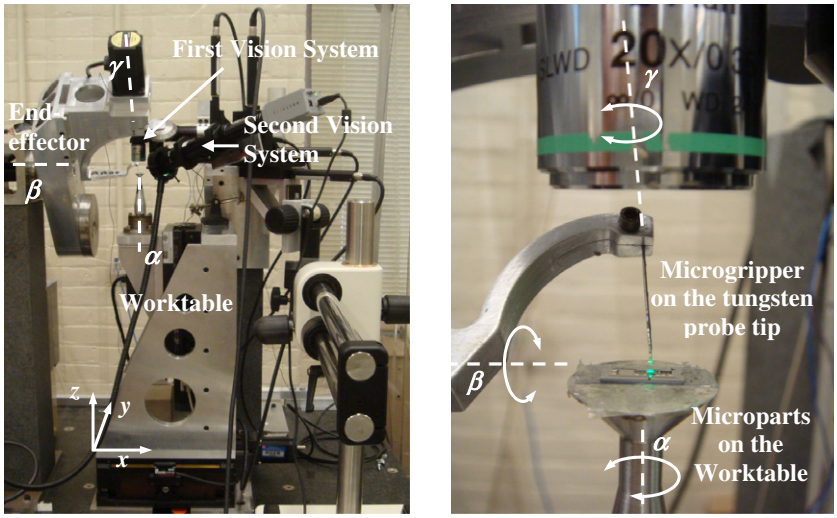

(*a*) (*b*)

Figure 1. (*a*) The in-house six-DOF manipulator; (*b*) a close-up of the manipulator.

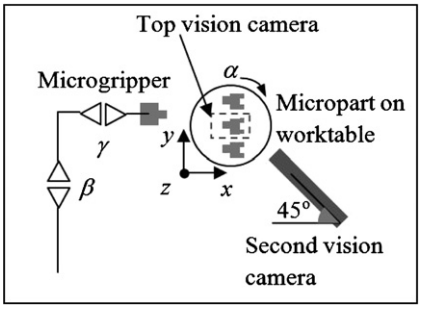

Figure 2. Schematic showing the location of the two vision cameras.

During the assembly process, the microgripper is bonded onto the tungsten probe, while the microparts are loaded onto the worktable. Stepper motor drivers are used to drive the translational and rotational motions of the manipulator with an accuracy of 0.2 μm and 0.072°. A complete description of the manipulator is reported in [21].

2.2. Vision system

Two vision CMOS cameras were installed onto the manipulator to fully monitor the microassembly process. The first camera is Pixelink model PL-A741 with 1.3 megapixels and it is configured to capture images from the top view. The second camera is Pixelink model PL-B776 with 3.0 megapixels and it is configured to capture from a trimetric perspective view. Both cameras were mounted on a motorized positioning stage so that the microgripper can be located and positioned within the camera view at the initial setup. The positioning stages were secured to a granite base and a boom stand. During the microassembly process, the two cameras remain stationary at the preset positions. The first vision system, having a top-view configuration, can provide visual information for the micropart grasping and alignment process. The second vision system, which is the primary focus of this paper, can provide the 3D information for the assembly process.

The initial configuration of the second camera is shown in figure 2. The camera is located approximately 45° between the *x*- and *y*-axes of the worktable and is inclined 15° with respect to the *xy* plane to capture the 3D image of the microgripper. To magnify the size of the micro-components in the images, the vision camera was connected to the Zoom125C optical system. The magnification of the optical system is set to 14.6×. With the selected CMOS camera, the available field of view is 330 μm × 440 μm and the depth of field is 24 μm [22]. A fiberoptic ringlight was attached to the system to illuminate the microassembly process.

2.3. Micro-components design

The microgripper and the micropart used in this experiment are shown in figure 3. A single-crystal silicon wafer 25 μm thick was selected as the structural material and these micro-components were fabricated using the SOIMUMPs

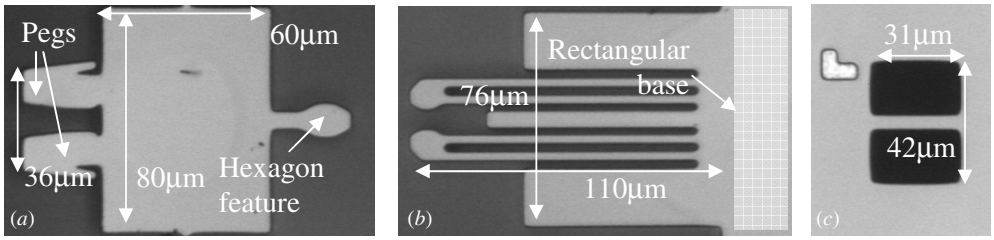

Figure 3. Images of (*a*) micropart, (*b*) microgripper and (*c*) slot, under the microscope.

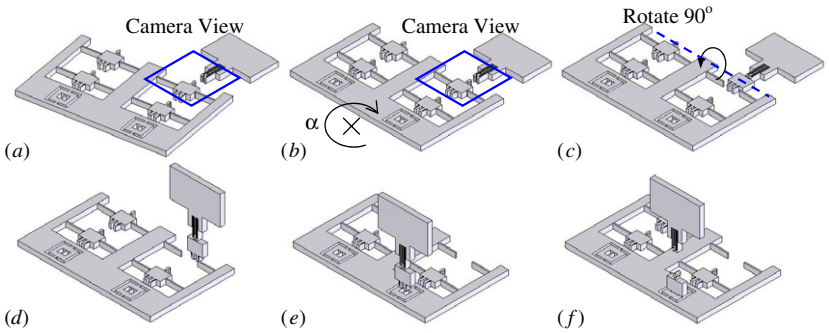

Figure 4. Schematics of the microassembly process: (*a*) the micropart is brought within the camera view; (*b*) the micropart rotates to the proper orientation for grasping; (*c*) the microgripper grasps and detaches the micropart; (*d*) the microgripper with the micropart remains at the same position after 90° rotation; (*e*) the worktable manipulates the slot underneath the micropart; (*f*) the microgripper inserts and then releases the micropart.

micromachining process. The microgripper, modified from the PolyMUMPs design by Dechev *et al* in [23], has dimensions 110 μm × 76 μm and it can be bonded onto the tungsten probe through the connecting rectangular base. A passive, snap-locking actuation mechanism was employed to control the grasping motion of the microgripper. During the microassembly process, the assembly force exerted by the micropart on the microgripper will force the gripper tips to open.

The micropart to be grasped has overall dimensions of 80 μm × 60 μm and it is supported on the substrate through two supporting tethers. A hexagon feature was incorporated on the micropart design to facilitate grasping by the passive microgripper. To ensure successful detachment of the micropart from the supporting tethers, the assembly force required to break the tethers must be higher than the force required to fully grasp the micropart. The assembly forces for each scenario were evaluated through finite element simulations. The detachment process was successfully conducted for the selected design parameters [17, 18].

Two pegs are designed on the other end of the micropart for the out-of-plane insertion operation. After 90° rotation, these pegs are to be inserted into the slot on the substrate. The perimeter of the slot is designed so that it can provide 3 μm clearance between the peg and the slot initially. When the pegs are gradually inserted into the slots, the width of the pegs increases from 36 to 42 μm to secure the micropart with the slots.

2.4. Overview of the microassembly process

To perform the microassembly process, the microgripper needs to be bonded onto the probe of the end-effector. A thin layer of the UV adhesive is applied onto the probe tip and the microgripper is positioned underneath the tip for curing. Details of the bonding process can be referenced to [18, 24]. The top-view camera then positions and focuses on the microgripper. Microparts are loaded onto the worktable and manipulated within the camera view as shown in figure 4(*a*). Since the micropart may not be aligned precisely with the microgripper to facilitate the grasping process, a dynamic tracking algorithm [19, 20] can be employed to automatically correct the orientation of the micropart through rotation from the worktable as shown in figure 4(*b*). Using the visual information from the top-view camera, the microgripper can visually guide to grasp the micropart and detach the micropart from the supporting substrate.

After the microgripper successfully grasps and detaches the micropart, the microgripper rotates 90° to prepare for the insertion operation as shown in figure 4(*c*). Since the tip of the probe lies on the axis of rotation, the microgripper with the micropart roughly remains at the same position after rotation. The worktable then manipulates to position the target slot for insertion operation. Based on the design layout of the chip, the position difference between the insertion slot and the micropart can be evaluated and the slot can be approximately positioned underneath the micropart. Visual images are used to precisely align the slot with the micropart for successful insertion as illustrated in figure 4(*f*).

2.5. Challenges in the microassembly process

The success of the above microassembly process relies on the precise alignment between the micropart and the slot. Chu *et al* in [18] described a two-stage alignment strategy through visual images from the top-view camera. The camera first positioned its focal plane at the tip of the micropart to estimate the edge of the micropart tip. Then the camera moved along the optical axis and focused on the slot. By projecting the estimated edge of the micropart tip onto the image, the slot can be manipulated and aligned with the micropart for the assembly. Nevertheless, locating the edge of the micropart tip is tedious. To improve the alignment, this work proposes a new alignment strategy through a second vision camera with a trimetric viewpoint. Once the micropart and the slot appear in the image after rotation, the slot is visually servoed to the micropart for the latter insertion operation.

2.6. Advantages of visual servoing through a single-vision camera

When performing the microassembly process, the unknown 3D position between the micropart and the slot must be evaluated from the visual images. To evaluate the 3D

position, one common practice is to use a stereo vision system [11, 25]. Through a triangulation algorithm, the images from the two cameras can be used to solve for the unknown position. However, one limitation of the stereo vision system is that the micropart and the slot must appear in both images. When a stereo vision system is used in the microassembly process, high magnification lenses are often required to magnify the micro-objects and hence the depth of the field is substantially decreased. Further, with two cameras located close to each other, the available workspace for the microassembly process is significantly reduced. If the two cameras are instead positioned at two different angles to observe the assembly process, the sensitivity as well as the available visual information for image processing can be maximized [12]. In this work, the 3D information is evaluated only from a single-vision camera through the use of the micropart reflection. The micropart reflection exists already in the visual image and hence does not require any special setup. Comparing to the stereo vision system, this approach only requires one set of visual images at a time and hence the processing time can be reduced.

2.7. Literature review on 3D visual servoing for microassembly

Over the past few years, visual servoing algorithms for use in the microassembly process have been proposed and examined by several research groups. Nevertheless, many of these algorithms are developed based on a robotic manipulator with a top-view camera configuration. Use of visual servoing algorithms for microassembly through trimetric-view images is still not often reported in the literature. Yasin *et al* [12] proposed to incorporate the CAD model to estimate the pose of the object within the image for tracking and manipulation. The CAD model of the object is first rendered and superimposed onto the image. Through iterations, the pose of the CAD model of the object is refined and matched with the actual object in the image. Experiments were conducted to track a square-shaped object (970 μm wide). The object was translated by a known displacement and the pose of the object at the new position was evaluated and compared to the commanded translation. When the object was translated by 300 μm, the error in the displacement evaluated from the change in the pose was found to be between 4 and 7 μm. When the translation is 20 μm, the evaluated displacement error is less than 1 μm. Tamadazte *et al* [13, 14] also used the CAD-model approach for the visual-based microassembly process. The process consists of inserting a micropart on top of another micropart and the micropart has dimensions of 400 μm $\times$ 400 μm $\times$ 100 μm. CAD models of the top and bottom microparts at their desired poses are first superimposed onto the image. Through the proposed algorithm, the top and the bottom of the microparts in the image are manipulated and matched with their poses in the CAD model, respectively. Experimental results show that the position error ranged from 0.29 to 3.52 μm and the micropart of interest was successfully assembled to the other micropart.

3. Development of the image Jacobian

3.1. Jacobian matrix

In image-based visual servoing, an object (or feature) from the image is required to be manipulated to a set of desired image coordinates. During the manipulation process, the controller inputs are developed through the visual information from the acquired images. In many papers on the subject, the Jacobian matrix (J) is defined as the matrix that relates the motions of a feature in the image to manipulator motions with respect to the camera frame. Let $s = [u, v]$ be the coordinates of the feature in the image. The velocities from the manipulator that contribute to the motions of the feature, $\dot{s}$, in consecutive images can be represented as [2]

$$\dot{s} = J\dot{p} \tag{1}$$

$$\begin{bmatrix} \dot{u} \\ \dot{v} \end{bmatrix} = \begin{bmatrix} \lambda/z_c & 0 & -u/z_c & -uv/\lambda & (\lambda^2+u^2)/\lambda & -v \\ 0 & \lambda/z_c & -v/z_c & -(\lambda^2+v^2)/\lambda & uv/\lambda & u \end{bmatrix} \times [\dot{x}_c, \dot{y}_c, \dot{z}_c, \dot{\omega}_{xc}, \dot{\omega}_{yc}, \dot{\omega}_{zc}]^T \tag{2}$$

where $\dot{p}$ denotes the translational and rotational velocities of the feature with respect to the camera frame, λ is the focal length of the vision system and z_c is the distance between the camera and the slot with respect to the camera frame.

As shown in equation (2), the motions of the feature in the image have only two degrees of freedom (DOF) and that is the change of the image coordinates. The feature itself can have up to six degrees of motion supplied by the manipulator. In this work, the feature to be tracked is the centroid of the slot on the worktable and the slot needs to be manipulated underneath the micropart. During the fabrication of the micro-components, the slot is fabricated so it will have the correct orientation for the insertion of the micropart, as shown in figure 4 previously. Hence, after 90° rotation, the slot does not require any rotation to adjust its orientation during the servoing. The slot only needs to be translated to the desired position through the three translation stages of the worktable. Hence, the Jacobian matrix for this work can be simplified as

$$J = \begin{bmatrix} \lambda/z_c & 0 & -u/z_c \\ 0 & \lambda/z_c & -v/z_c \end{bmatrix}. \tag{3}$$

Let the desired image coordinates, $s_{\text{desired}} = [u_{\text{desired}}, v_{\text{desired}}]$, that the slot needs to be manipulated be the peg on the micropart. During the assembly process, the micropart or these desired image coordinates remain stationary in the image. Then, the control objective is to minimize the coordinate differences between the micropart and the slot by moving the image coordinates of the slot to the desired coordinates. The required velocities that move the slot to the micropart become

$$\begin{bmatrix} \dot{x}_c \\ \dot{y}_c \\ \dot{z}_c \end{bmatrix} = J_p^{-1} \cdot [s_{\text{desired}} - s_{\text{current}}] \tag{4}$$

where J_p^{-1} is the pseudoinverse of J.

Since the developed Jacobian matrix is not a square matrix, the pseudoinverse method is used to estimate the inverse of the matrix. For an $m \times n$ matrix with $m < n$, the pseudoinverse is [2]

$$J_P^{-1} = (J^T J)^{-1} J^T. \tag{5}$$

The above velocities needed to complete the servoing part are developed with respect to the camera frame. Since the controller inputs for the manipulator need to be computed in its robot frame (x_r, y_r, z_r), transformation is needed to express the equivalent velocities in the robot frame. Assume that the robot frame of the manipulator can be transformed to the frame of the camera through a rotational matrix, R; the required controller inputs for the manipulator become

$$\begin{aligned}\begin{bmatrix}\dot{x}_r\\ \dot{y}_r\\ \dot{z}_r\end{bmatrix} &= R(\alpha,\beta,\gamma)\cdot\begin{bmatrix}\dot{x}_c\\ \dot{y}_c\\ \dot{z}_c\end{bmatrix}\\ &= R(\alpha,\beta,\gamma)\cdot J_p^{-1}\cdot[s_{\text{desired}} - s_{\text{current}}].\end{aligned} \tag{6}$$

3.2. Model-free visual servoing

When constructing the Jacobian matrix, prior knowledge of the intrinsic and extrinsic parameters of the vision system is required, and these parameters can be evaluated through system calibration. In this work, the vision system is first adjusted so that the micropart lies on the focal plane and the system then remains stationary after setup. Manipulation of the slot is performed within the depth of field of the vision system. Since the z_c distance between the camera and the slot changes during the manipulation, the Jacobian matrix will not be constant. In addition, these system parameters are either not known or difficult to evaluate precisely. Hence, the Jacobian matrix can be evaluated experimentally. This approach is also known as model-free visual servoing. To date, many research groups have proposed various methodologies to estimate the Jacobian matrix on-line, and these include the local least-squares (LLS) estimation [26], recursive least-squares (RLS) estimation [27, 28], or Kalman filtering [9, 16]. When evaluating the Jacobian matrix, the rotational matrix can be integrated into the Jacobian matrix and so it does not have to be evaluated separately.

3.2.1. Jacobian matrix from the last move. One method to estimate the Jacobian matrix is the 'last move approach' by Sebastian *et al* in [29]. Assume that the manipulator is commanded to manipulate through a series of movements. The changes in the image coordinates of the feature are all recorded. The Jacobian matrix of the system, after n movements, can be approximated as

$$\begin{bmatrix}\Delta s_1\\ \vdots\\ \Delta s_n\end{bmatrix} = \begin{bmatrix}\Delta x_{r,1} & \Delta y_{r,1} & \Delta z_{r,1}\\ & \vdots & \\ \Delta x_{r,n} & \Delta y_{r,n} & \Delta z_{r,n}\end{bmatrix} J^T. \tag{7}$$

3.2.2. RLS estimation. Hosoda *et al* in [27] proposed a recursive least squares estimation with data weighting algorithm for the Jacobian estimation. When adopting the recursive approach, an initial Jacobian matrix needs to be declared. In this work, an initial Jacobian matrix can first be determined using the above method and then the Jacobian matrix continues to refine after the subsequent movements. The new Jacobian matrix becomes

$$J_{k+1} = J_k + \frac{(\Delta s_k - J_k \Delta q_k)\Delta q_k^T P_k}{\rho + \Delta q_k^T P_k \Delta q_k} \tag{8}$$

where ρ is the forgetting factor and P_k is the covariance matrix.

A forgetting factor of value between 0 and 1 can be chosen. If ρ is equal to 1, the new information is averaged with the previous data. If ρ is less than 1, previous data are weighted less in the Jacobian estimation. The covariance matrix P_k can be evaluated using the equation

$$P_{k+1} = \frac{1}{\rho}\left(P_k - \frac{P_k \Delta q_k \Delta q_k^T P_k}{\rho + \Delta q_k^T P_k \Delta q_k}\right). \tag{9}$$

3.3. Multiple feature tracking

When performing the image-based visual servoing, the image coordinates, having a dimension 2, are used to evaluate the required three translational inputs of the manipulator through the Jacobian matrix. As discussed in the earlier section, there exist infinite possible translational inputs that could position the feature to particular image coordinates. To position the feature to the desired 3D positions, one approach is to add more constraints to the system by tracking two or multiple features simultaneously. The Jacobian matrix of the vision system is equivalent to the Jacobian matrices of multiple features stacking together [29, 30]:

$$\begin{aligned}&\begin{bmatrix}\Delta s_{\text{feature }1,1} & \Delta s_{\text{feature }2,1} & \cdots & \Delta s_{\text{feature }m,1}\\ & \vdots & & \\ \Delta s_{\text{feature }1,n} & \Delta s_{\text{feature }2,n} & \cdots & \Delta s_{\text{feature }m,n}\end{bmatrix}\\ &= \begin{bmatrix}\Delta x_{r,1} & \Delta y_{r,1} & \Delta z_{r,1}\\ & \vdots & \\ \Delta x_{r,n} & \Delta y_{r,n} & \Delta z_{r,n}\end{bmatrix}\begin{bmatrix}J^T_{\text{feature }1}\\ J^T_{\text{feature }2}\\ \vdots\\ J^T_{\text{feature }n}\end{bmatrix}.\end{aligned} \tag{10}$$

These features being selected must move independently in the image and must not be aligned. However, the possible features in the MEMS structure are relatively two dimensional. For instance, the slot on the worktable is the feature to be tracked and the image coordinates of the three corners are selected as the three distinctive feature points to be tracked. During the manipulation process, the changes in these features are linearly dependent and hence the evaluated Jacobian matrix could be inaccurate. Figure 5(*a*) shows an example where the slot is desired to be servoed to the points on the microparts. As shown in figure 5(*b*), a Jacobian matrix was evaluated using the visual feedback from three corners. Despite the fact that the slot appears to be aligned with the micropart from the camera view, the slot is actually misaligned in all three coordinate directions.

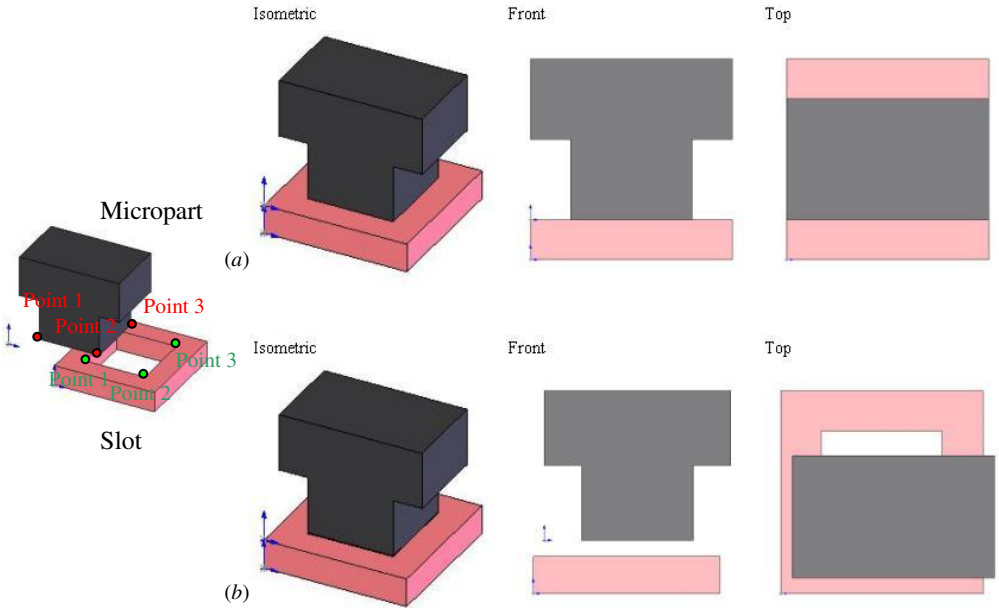

Figure 5. (*a*) Using the correct Jacobian matrix to align the slot with the micropart; (*b*) using an inaccurate Jacobian matrix to virtually align the slot with the micropart.

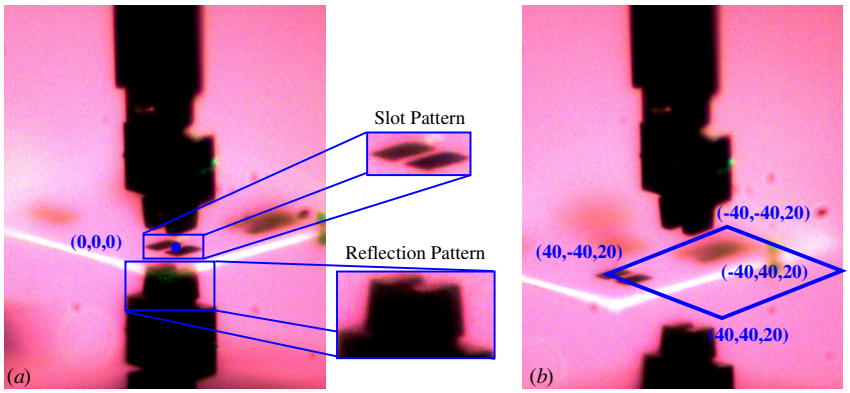

Figure 6. Image from the trimetric-view camera: (*a*) the slot at the desired position; (*b*) the slot at an arbitrary position.

3.4. Feature selection

Since the corners of the slot are not sufficient to evaluate the 3D positions for alignment, this work also included the reflection of the micropart from the mirror as an additional feature. To identify these features in the image, a pattern-matching algorithm was employed to locate these features in successive visual images. The slot and the micropart reflection are selected as the two features for tracking, as shown in figure 6. Initially, each individual feature was first declared in the image by drawing a region of interest enclosed as the template. During the process, the algorithm scanned through the captured image with a search window to compute the correlation value. The coordinates of the window which had the highest correlation value with each feature template were identified as the visual position of such a feature. Figure 6 shows an image obtained from the trimetric-view camera.

3.5. Control algorithm for visual servoing

The evaluated Jacobian matrix was used to compute the required controller inputs of the manipulator. The manipulator stepper motors are configured to manipulate the worktable along the three axes, based on the specified displacement inputs. During each sample interval, the image coordinates of the two features were evaluated from the newly captured image to update the controller inputs. A proportional gain, K, was added to the controller inputs to improve the robustness and the discrete displacement inputs for the motors become

$$\begin{bmatrix} \Delta x_r \\ \Delta y_r \\ \Delta y_z \end{bmatrix} = K \cdot J_p^{-1} \cdot [s_{\text{desired}} - s_{\text{current}}]. \tag{11}$$

This visual servoing scheme continues until the evaluated displacement inputs are less than 0.2 μm, which is the minimum resolution of the stepper motors.

Table 1. Positions of the slot and the calibration steps for each set of the experiment.

	X (μm)	Y (μm)	Z (μm)	Steps 1, 4, 7	Steps 2, 5, 8	Steps 3, 6, 9	New X (μm)	New Y (μm)	New Z (μm)
Set 1 Set 2	40	40	20	(5, 0, 0)	(0, 5, 0)	(0, 0, 5)	25	25	5
Set 3 Set 4	−40	40	20	(−5, 0, 0)	(0, 5, 0)	(0, 0, 5)	−25	25	5
Set 5 Set 6	40	−40	20	(5, 0, 0)	(0, −5, 0)	(0, 0, 5)	25	−25	5
Set 7 Set 8	−40	−40	20	(−5, 0, 0)	(0, −5, 0)	(0, 0, 5)	−25	−25	5

4. Experiments

4.1. Estimation of the Jacobian matrix

Using the micropart reflection as an additional tracking feature, the system Jacobian matrix was evaluated experimentally and used to compute the position differences between the slot and the micropart. Before the experiment, the slot was first manipulated underneath the micropart to create the learning image as shown in figure 6. The micropart is roughly 20 μm above the slot so that both patterns can be clearly located. From the learning image, the desired image coordinates of the slot and the micropart reflection were evaluated and recorded. Then, the slot was manipulated to four different locations, 40 μm away from the desired position and 20 μm farther underneath the micropart for the experiments. Two trials were conducted at each location to examine the accuracy and repeatability of the position evaluation. The Jacobian matrix for each set was evaluated through nine calibration steps of movements at an increment of 5 μm toward the micropart. For the recursive approach, information from the first three steps is used to construct the initial Jacobian matrix and the remaining six steps are used to refine the matrix. At each step, only one axis was manipulated and the inputs of the nine steps are summarized in table 1. After each step, images from the camera were captured and the image coordinates of the two features were evaluated. To minimize the noise during image acquisition, five consecutive images, roughly 1 s apart, were taken and the average image coordinates were employed to evaluate the Jacobian matrix. The position differences between the slot at the current position and the desired position were then computed accordingly.

The required displacement inputs using the Jacobian estimation from the last move approach are summarized in table 2 and required displacement inputs with the recursive approach are summarized in table 3. Different forgetting factors and initial variable of the covariance matrix were examined and table 3 shows the results using $\rho = 0.9$ and

$$P = \begin{bmatrix} 1 & 0.5 & 0.5 \\ 0.5 & 1 & 0.5 \\ 0.5 & 0.5 & 1 \end{bmatrix}.$$

Results from the experiment showed that both Jacobian estimation schemes can be implemented to determine the unknown Jacobian matrix of the system for the given workspace. From the evaluated Jacobian matrix, the position error in the xy plane is determined to be within 3.6 μm, while the error in the z-direction is less than 1.1 μm. A higher forgetting value would provide a better evaluation in the position. When reducing the forgetting value from 0.9 to 0.5, the position error can be increased to 4.5 μm. Changing the initial value of the covariance matrix does not have a significant influence on the evaluation process as the covariance matrix will gradually converge to its value through enough iteration.

When comparing the evaluated positions for each pair at the same location, the scale of the position error varied from one to the other but the variation is generally within 2 μm. For instance, the error for the x-position evaluated in the first set using the recursive approach is 2.2 μm, but the error in the second set is only 0.6 μm. Hence, the proposed position evaluation scheme can achieve high repeatability. Based on the measurement data obtained from the captured images, deviations in the evaluated image coordinates of the features are suspected to be the repeatability errors in the position evaluation. For the five images captured at the same

Table 2. The required displacement inputs and the errors when using the last move approach.

	X	$\lvert \Delta X \rvert$	Y	$\lvert \Delta Y \rvert$	Z	$\lvert \Delta Z \rvert$
Set 1	24.25	0.75	22.48	2.52	4.44	0.56
Set 2	26.43	1.43	22.37	2.63	4.42	0.58
Set 3	−24.12	0.88	21.53	3.47	4.34	0.66
Set 4	−23.98	1.02	23.12	1.88	4.54	0.46
Set 5	26.35	1.35	−24.95	0.05	4.06	0.94
Set 6	25.59	0.59	−23.19	1.81	4.7	0.3
Set 7	−23.7	1.3	−25.21	0.21	4.16	0.84
Set 8	−23.37	1.63	−24.84	0.16	4.3	0.7

Table 3. The required displacement inputs and the errors when using the recursive approach.

	X	$\lvert \Delta X \rvert$	Y	$\lvert \Delta Y \rvert$	Z	$\lvert \Delta Z \rvert$
Set 1	22.83	2.17	22.44	2.56	4.35	0.65
Set 2	25.57	0.57	21.39	3.61	4.41	0.59
Set 3	−23.39	1.61	21.62	3.38	4.41	0.59
Set 4	−23.82	1.18	22.82	2.18	4.56	0.44
Set 5	26.29	1.29	−24.26	0.74	3.88	1.12
Set 6	24.45	0.55	−22.18	2.82	4.77	0.23
Set 7	−23.41	1.53	−25.1	0.1	3.98	1.02
Set 8	−23.65	1.35	−24.44	0.56	4.34	0.66

Table 4. Positions of the slot and the calibration steps for each set of the experiment.

	X (μm)	Y (μm)	Z (μm)	Steps 1, 4, 7	Steps 2, 5, 8	Steps 3, 6, 9	New X (μm)	New Y (μm)	New Z (μm)
Exp 1	−28	17	24	(−5, 0, 0)	(0, 5, 0)	(0, 0, 5)	−13	2	9
Exp 2	10	15	30	(5, 0, 0)	(0, −5, 0)	(0, 0, 5)	−5	30	15
Exp 3	10	−10	5	(−5, 0, 0)	(0, 5, 0)	(0, 0, −5)	25	−25	20

Table 5. Position errors after the visual servoing process.

		Iteration	X	$\lvert \Delta X \rvert$	Y	$\lvert \Delta Y \rvert$	Z	$\lvert \Delta Z \rvert$
Exp 1 ($K = 0.5$)	Last move	6	−13.2	0.2	3.0	1	8.6	0.4
	Recursive ($\rho = 0.9$)	8	−13.6	0.6	2.6	0.6	9.2	0.2
	Recursive ($\rho = 0.5$)	6	−12.6	0.4	2.8	0.8	8	1
Exp 2 ($K = 0.5$)	Last move	6	−3.6	1.4	29.2	0.8	12.4	2.6
	Recursive ($\rho = 0.9$)	9	−4.8	0.2	29.6	0.4	14.8	0.2
	Recursive ($\rho = 0.5$)	7	−4.4	0.6	29	1	14.6	0.4
Exp 3 ($K = 0.5$)	Last move	7	24.6	0.4	−24.6	0.4	19.4	0.6
	Recursive ($\rho = 0.9$)	7	25.2	0.2	−25.6	0.8	19.8	0.2
	Recursive ($\rho = 0.5$)	6	24.4	0.6	−24.4	0.6	19	1

location, the evaluated image coordinates of the features using the pattern matching technique varied by roughly 3 to 5 pixels. This error is mainly due to the quality of the captured images and the influence of noise during image acquisition. When the slot was manipulated to a new position, the features appearing in the images were not identical to the supplied templates and the quality of the captured images had greater influence on evaluating the coordinates.

To justify the above claim, an experiment was conducted to determine the performance of the coordinate evaluation process. One hundred images were captured at the same location and the coordinates of the features were then evaluated. When the slot was positioned exactly at the same position where the templates were created, the variation between the evaluated coordinates was less than 1 pixel and the standard deviation was less than 0.4 pixels. Once the slot was manipulated to an arbitrary position, the variation between the evaluated coordinates increased to 5 pixels and the standard deviation increased to 2 pixels. Hence, factors such as brightness and the feature sharpness contributed to the image quality, affecting the coordinate evaluation process.

4.2. Visual servoing for microassembly

The visual servoing scheme for the microassembly process was examined using the Jacobian matrix estimated from the two methods. Three experiments were conducted to evaluate the servoing performance. The first experiment was to complete the servoing process after the nine calibration steps were carried out as previously described. These nine calibration steps were chosen to move the slot toward the desired location. Hence, the estimated Jacobian matrix initially would be close to the true Jacobian matrix.

During the experiment, these calibration steps can be selected as needed since the distance between the slot and the desired location was known. When performing the actual microassembly process in an unknown environment, these calibration steps for each axis have to be judged from the 2D visual image and hence the selected calibration steps may not necessarily move the slot toward the desired location. Hence, the impact of the uncertainty in the initial Jacobian matrix on the servoing performance must be evaluated. In the second experiment, intentional errors were introduced during the calibration procedure. The calibration steps for the x- and z-axes were chosen similarly and the slot can be moved toward the desired location. However, the calibration process for the y-axis was altered so that the insertion slot was located further away from the desired location in the y-axis direction. This experiment could then evaluate whether or not the calibration error for the y-axis would result in more position error as compared to the other two axes.

In the last experiment, the worst-case scenario was considered and a poor initial Jacobian matrix was adopted for visual servoing. These nine calibration steps were altered to move the slot away from the desired location in all axis directions and the initial Jacobian matrix thus estimated would not be close to its true value. The position error and the number of iterations for convergence were evaluated and compared with the previous experiments.

For each experiment, the last move approach and the recursive approach with $\rho = 0.9$, and with $\rho = 0.5$ for Jacobian matrix estimation, were examined. To gradually guide the slot toward the desired location during the visual servoing process, the proportional gain value of the manipulator controller was set between 0 and 1. In this experiment, the proportional gain was set to 0.5. If a higher proportional gain were adopted, fewer iterations would be required to reach the desired location. However, during visual servoing, the slot position could overshoot in the z-direction resulting in damage to the micropart or the microgripper.

The initial positions of the slot and the chosen calibration steps are listed in table 4. Experimental results show that all visual servoing schemes can be used to perform the microassembly process as summarized in table 5. After six to nine iterations, the slot was servoed and placed properly underneath the micropart for part insertion. The errors between the controller inputs and the actual positions were

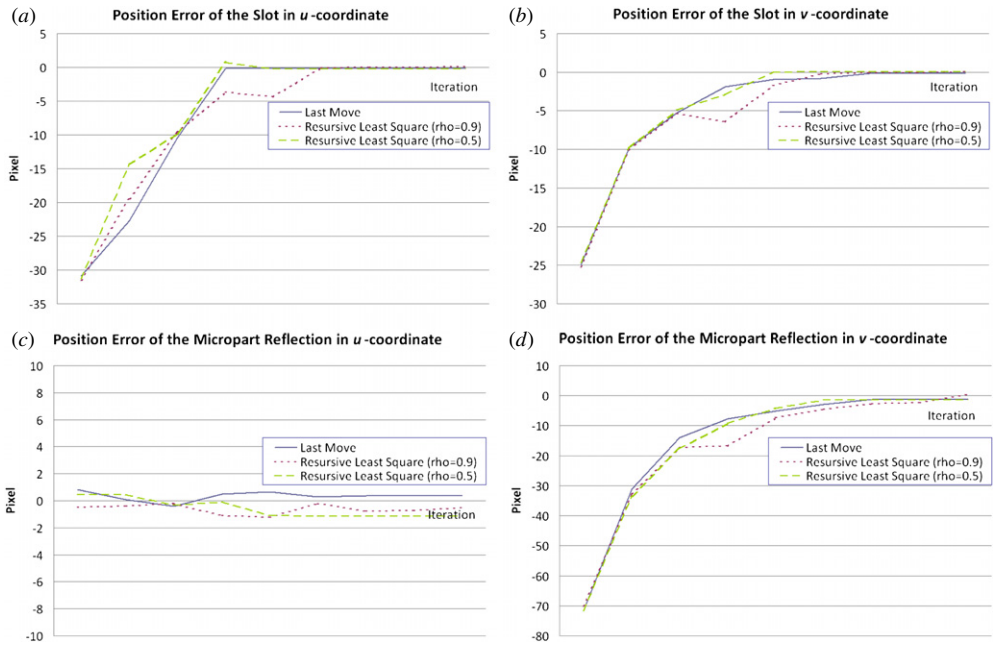

Figure 7. Errors in the image coordinates of (*a*) slot (*u*-coordinate), (*b*) slot (*v*-coordinate), (*c*) reflection (*u*-coordinate), (*d*) reflection (*v*-coordinate), during visual servoing.

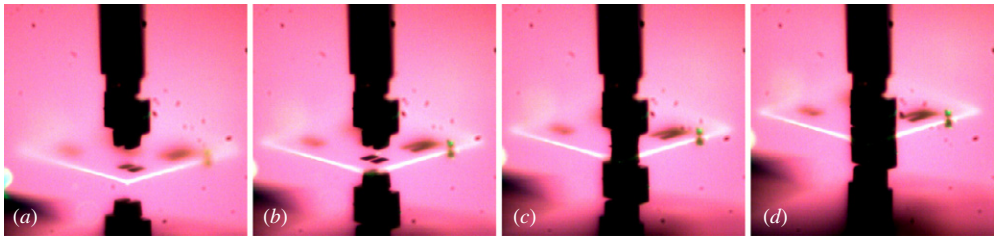

Figure 8. (*a*) The initial position of the slot after nine calibration steps; (*b*) the slot was servoed to the desired location; (*c*) the slot was raised to the tip of the micropart; (*d*) the micropart was successfully inserted into the slot.

Table 6. Position errors with different proportional gains.

		Iteration	X	$\|\Delta X\|$	Y	$\|\Delta Y\|$	Z	$\|\Delta Z\|$
Exp 1 ($K = 0.2$)	Last move	17	−12.2	0.8	1.4	0.6	9	0
	Recursive ($\rho = 0.9$)	17	−12.6	0.4	1.4	0.6	8.4	0.6
	Recursive ($\rho = 0.5$)	12	−11.8	1.2	2.2	0.2	7.6	1.4
Exp 1 ($K = 0.8$)	Last move	3	−12.8	0.2	2	0	9.6	0.6
	Recursive ($\rho = 0.9$)	3	−13.2	0.2	2	0	9.4	0.4
	Recursive ($\rho = 0.5$)	3	−13	0	1.8	0.2	9	0

roughly within 1 μm. The image coordinates of the two features in the final image were within 2.5 pixels of the desired coordinates. Figure 7 shows the errors in the image coordinates of the two features during the servoing process for the first experiment. After the servoing part was completed, the slot was then moved upward for the insertion operation. Since the peg of the micropart has the edges tapered to provide clearances for assembly, the micropart at each experiment is inserted successfully into the slot. Figure 8 illustrates the process flow of the microassembly experiment.

To examine the influence of different gain values, the proportional gain, K, in the first experiment was set to 0.2 and 0.8. Experimental results show that for both gain values, the errors were still roughly within 1 μm and similar to $K = 0.5$ as summarized in table 6. However, the number of iterations increased to 17 for $K = 0.2$ and reduced to 3 for $K = 0.8$.

When compared with the position error of the slot evaluated in the second experiment, the error in the y-axis is similar to other two axes, and is not necessarily higher. In the third experiment, the position errors are also comparable to the first two experiments. Hence, the servoing performance for each Jacobian estimation scheme is robust to the quality of the initial Jacobian matrix. The initial Jacobian matrix can be constructed using any calibration steps as the Jacobian matrix can be refined to its true value after iterations and the computed controller can move the slot to the desired position with high

accuracy. Experimental results also show that the quality of the initial Jacobian matrix does not have a direct impact on the number of iterations for convergence.

5. Conclusion and future work

An image-based visual servoing algorithm had been developed to assist in the process of microassembly. A single-vision camera with a trimetric-view configuration was used to provide visual information on the process. In this paper, the technique of the last move approach and the recursive least-squares approach were used to evaluate the Jacobian matrix of the uncalibrated manipulator. To evaluate the position differences between the slot and the micropart, the reflection of the micropart from the substrate was tracked as an additional feature in the servoing process. Experimental results showed that both Jacobian estimation approaches with the inclusion of the micropart reflection can be used to correctly evaluate the position differences with an accuracy of 3.6 μm. By applying a proportional gain to the controller inputs, this accuracy can be improved to within 1 μm. Based on the results from each equivalent pair, measurement noises from the captured images mainly contribute to the errors in evaluating the position. To filter out the noise, more images should be captured at each step to minimize the effect of the outliers and the fluctuation.

The calibration steps used to construct the initial Jacobian matrix can be chosen arbitrarily as the estimated Jacobian matrix will gradually converge to the true Jacobian matrix after sufficient iterations. Hence, neither the servoing performance nor the convergence rate will be affected due to the poor estimation of the initial Jacobian matrix.

Three-dimensional visual servoing for use in microassembly processes is important for the development of 3D microdevices. With this visual servoing scheme, the alignment process between the micropart and the slot can be performed with high accuracy and repeatability. This scheme does not require any prior knowledge of the vision system or the CAD-model reconstruction and the slot at an arbitrary position initially can be successfully servoed to the desired position for the assembly. With the camera at a trimetric view, more visual information can be acquired and more complex microparts may be assembled. Hence, this configuration can provide more manufacturing flexibility than the common top-view microassembly processes. The next phase of this ongoing research is to implement this visual servoing scheme for multiple micropart assemblies. Construction of a high aspect-ratio microcoil is under development.

When conducting the visual servoing experiments, instability was not experienced in any of the experimental trials. The slot at various locations was successfully manipulated to the desired location and the controller inputs in x, y and z gradually converged to a value below 0.2 μm, which is the minimum resolution of the actuator motors. Since stability is an important issue in visual servoing, a detailed investigation will be conducted as part of our future work.

Acknowledgment

The authors would like to thank CMC Microsystems for partial support for MEMS chip fabrication.

References

[1] Bohringer K F, Fearing R S and Goldberg K Y 1999 *Microassembly Handbook of Industrial Robotics* 2nd edn, ed S Y Nof (New York: Wiley) pp 1045–6

[2] Hutchinson S, Hager G D and Corke P I 1996 A tutorial on visual servo control *IEEE Trans. Robot. Autom.* **12** 651–70

[3] Martinet P and Gallice J 1999 Position based visual servoing using a non linear approach *Proc. IEEE Int. Conf. on Intelligent Robots and Systems* pp 531–6

[4] Marchand E, Chaumetter F and Spindler F 2002 Controlling an uninstrumented manipulator by visual servoing *Int. J. Robot. Res.* **21** 635–41

[5] Corke P I and Hutchinson S A 2001 A new partitioned approach to image-based visual servoing *IEEE Trans. Robot. Autom.* **17** 507–15

[6] Feddema J T and Simon R W 1998 Microassembly of micro-electro-mechanical systems (MEMS) using visual servoing *The Confluence of Vision and Control (Lecture Notes in Control and Information Sciences* vol 237*)* (Berlin: Springer) pp 257–72

[7] Feddema J T and Simon R W 1998 Visual servoing and CAD-driven microassembly *IEEE Robot. Autom. Mag.* **5** 18–24

[8] Ralis S J, Vikramaditya B and Nelson B J 2000 Micropositioning of a weakly calibrated microassembly system using coarse-to-fine visual servoing strategies *IEEE Trans. Electron. Packag. Manuf.* **23** 123–31

[9] Wang J, Liu A, Tao X and Cho H 2007 Microassembly of micro peg and hole using uncalibrated visual servoing method *Precis. Eng.* **32** 173–81

[10] Mure-Dubois J and Hugli H 2006 Embedded 3D vision system for automated micro-assembly *Proc. SPIE* **6382** 6382J-1–10

[11] Sano T, Nagahata H and Yamamoto H 1999 Automatic micromanipulation system using stereoscopic microscope *Instrumentation and Measurement Technology Conf.* pp 327–31

[12] Yesin K B and Nelson B J 2005 A CAD model based tracking system for visually guided microassembly *Robotica* **23** 409–18

[13] Tamadazte B, Arnould T, Dembele S, Le Fort-Piat N and Marchand E 2009 Real-time vision-based microassembly of 3D MEMS *Proc. IEEE/ASME Int. Conf. on Advanced Intelligent Mechatronics* pp 88–93

[14] Tamadazte B, Marchand E, Dembele S and Le Fort-Piat N 2010 CAD model-based tracking and 3D visual-based control for MEMS microassembly *Int. J. Robot. Res.* **29** 1416–34

[15] Mikawa M, Yoshida K, Kubota M and Morimitsu T 1996 Visual servoing for micro mass axis alignment device *IEEE Int. Conf. Intelligent Robots and Systems* vol 3 pp 1091–6

[16] Kulpate C, Mehrandezh M and Paranjape R 2005 An eye-to-hand visual servoing structure for 3D positioning of a robotic arm using one camera and a flat mirror *Proc. IEEE Int. Conf. on Intelligent Robots and Systems* pp 1464–70

[17] Chu H K, Mills J K and Cleghorn W L 2009 Microgripper design for use in parallel microassembly processes *Proc. 2nd Microsystem and Nanoelectronics Research Conf.* pp 61–4

[18] Chu H K, Mills J K and Cleghorn W L 2010 Parallel microassembly with a robotic manipulation system *J. Micromech. Microeng.* **20** 125027

[19] Chu H K, Mills J K and Cleghorn W L 2010 Dynamic tracking of moving objects in microassembly through visual servoing *Proc. IEEE Int. Conf. on Mechatronics and Automation* pp 1738–43

[20] Chu H K, Mills J K and Cleghorn W L 2010 Automatic micropart re-orientation through visual tracking for

automated micro-assembly *Proc. ASME Int. Mechanical Engineering Congress and Exposition* p IMECE2010-38999

[21] Dechev N, Cleghorn W L and Mills J K 2006 Development of a 6 DOF robotic micromanipulator for use in 3D MEMS microassembly *Proc. IEEE Int. Conf. on Robotics and Automation* pp 281–8

[22] *Optem Zoom 125C Manual*, Thales Optem Inc., pp 1–8. Available at http://www.linos.com/pages/mediabase/original/Optem_Z125C_QIS_6773.pdf

[23] Dechev N, Cleghorn W L and Mills J K 2004 Microassembly of 3D microstructures using a compliant, passive microgripper *J. Microelectromech. Syst.* **13** 176–89

[24] Wang L, Mills J K and Cleghorn W L 2008 Automatic microassembly using visual servo control *IEEE Trans. Electron. Packag. Manuf.* **31** 316–25

[25] Martinet P and Cervera E 2001 Stacking Jacobians properly in stereo visual servoing *Proc. IEEE Int. Conf. on Robotics and Automation* pp 717–22

[26] Farahmand A M, Shademan A and Jagersand M 2007 Global visual-motor estimation for uncalibrated visual servoing *Proc. IEEE/RSJ Int. Conf. on Intelligent Robots and Systems* pp 1969–74

[27] Piepmeier J A, McMurray G V and Lupkin H 2004 Uncalibrated dynamic visual servoing *IEEE Trans. Robot. Autom.* **20** 143–7

[28] Hosoda K and Asada M 1994 Versatile visual servoing without knowledge of true Jacobian *Proc. IEEE Int. Conf. on Robotics and Automation* pp 186–93

[29] Sebastian J M, Pari L, Gonzalez C and Angel L 2005 A new method for the estimation of the image Jacobian for the control of an uncalibrated joint system *Pattern Recognition and Image Analysis (Lecture Notes in Computer Science* vol 3522*)* (Berlin: Springer) pp 631–8

[30] Nelson B, Papanikolopoulos N P and Khosla P K 1993 Visual servoing for robotic assembly *Visual Servoing: Real Time Control of Robot Manipulators Based on Visual Sensory Feedback* ed K Hashimoto *(World Scientific Series in Robotics and Automated Systems* vol 7*)* (Singapore: World Scientific) pp 139–64